# Mechanisms of Lead (II) Phycoremediation Using Scenedesmus Obliquus: Cell Physicochemical Properties, Biochemical Composition and Metabolomic Profiling

**Danouche M.** ( mohammed.danouche@usmba.ac.ma )
Moroccan Foundation for Advanced Science https://orcid.org/0000-0003-1654-8372
**El Ghachtouli N**
Sidi Mohamed Ben Abdellah University
**Aasfar A**
Moroccan Foundation for Advanced Science
**Bennis I.**
Moroccan Foundation for Advanced Science
**El Arroussi H.**
Moroccan Foundation for Advanced Science

**Research**

**Keywords:** Scenedesmus obliquus, Pb(II)-phycoremediation mechanism, Cells physicochemical properties, Biochemical composition, Metabolomic profiling.

**Posted Date:** July 9th, 2021

**DOI:** https://doi.org/10.21203/rs.3.rs-679604/v1

# Mechanisms of lead (II) phycoremediation using *Scenedesmus obliquus*: cell physicochemical properties, biochemical composition and metabolomic profiling

Danouche M.[a, b]*, El Ghachtouli N.[b], Aasfar A.[a], Bennis I.[a], El Arroussi H.[a,c]

[a] Green Biotechnology Center, Moroccan Foundation for Advanced Science, Innovation and Research (MAScIR), Rabat, Morocco.

[b] Microbial Biotechnology and Bioactive Molecules Laboratory, Sciences and Technologies Faculty, Sidi Mohamed Ben Abdellah University, Fez, Morocco.

[c] AgroBioScience (AgBS), Mohammed VI Polytechnic University (UM6P), Ben Guerir, Morocco.

***Corresponding author**:

Phone: +212 633 541 908

E-mail: mohammed.danouche@usmba.ac.ma (Danouche), h.elarroussi@mascir.ma (El Arrousi)

**Abstract**

This study highlights the mechanisms involved in Pb(II)-phycoremediation using the Pb(II) tolerant strain of *Scenedesmus obliquus*. Firstly, monitoring of cell growth kinetics in control and Pb(II)-doped medium revealed a significant growth inhibition, while the analyses through flow cytometry and Zetasizer revealed no difference in cell viability and size. Residual weights of control and Pb(II)-loaded cells assessed by thermogravimetric analysis, were 31.34% and 57.8%, respectively, indicating the uptake of Pb(II) into *S. obliquus* cells. Next, the use of chemical extraction to distinguish between the intracellular and extracellular uptake indicated the involvement of both biosorption (85.5%) and bioaccumulation (14.5%) mechanisms. Biosorption interaction of the cell wall and Pb(II) was confirmed by SEM, EDX, FTIR, zeta potential, zero-charge pH, and contact angle analyses. Besides, the biochemical characterization of control and

Pb(II)-loaded cells revealed that the bioaccumulation of Pb(II) induces significant increases in the carotenoids and lipids content and decreases in the proportions of chlorophyll, carbohydrates, and proteins. Finally, the metabolomic analysis indicated an increase in the relative abundance of fatty acid methyl esters, alkanes, aromatic compounds, and sterols. However, the alkenes and monounsaturated fatty acids decreased. Such metabolic adjustment may represent an adaptive strategy, that preventing high Pb(II)-bioaccumulation in cellular compartments.

**Keywords**: *Scenedesmus obliquus*; Pb(II)-phycoremediation mechanism; Cells physicochemical properties; Biochemical composition; Metabolomic profiling.

## Introduction

Since the formation of the Earth, nearly all of the heavy metals (HMs) that we know today have been naturally present in trace amounts and have been recycled biogeochemically between the environmental compartments (Garrett 2000). However, with global expansion, anthropogenic activities, including mining, excessive use of fertilizers in agriculture, and mismanagement of hazardous wastes, have resulted in an increase of the inorganic pollution of water and soil (Ashraf et al. 2014). Because they are not biodegradable, HMs can persist in ecosystems and can bioaccumulate into organisms of different trophic levels, causing various signs of toxicity to all life forms, including humans (Yan et al. 2018). Mercury (Hg(II)), cadmium (Cd(II)), lead (Pb(II)), arsenic (As(III)), and chromium (Cr(VI) are recognized as the most harmful pollutants (Kumar et al. 2015). The maximum contamination limits of these metals are 0.002, 0.005, 0.015, 0.01, and 0.1 mg $L^{-1}$, respectively (USEPA 2016). Unfortunately, their actual concentrations in industrial effluents generally exceed these standards requiring an adequate treatment before their release into the environment (Selvi et al. 2019). Thus, the exposure to Pb(II) results in a wide range of toxic effects on the physiological, biochemical and metabolic functions of exposed organisms (microorganisms, aquatic plants and animals), as well as human health complications resulting

from direct exposure or consumption of contaminated food or water (Lee et al. 2019). Indeed, various techniques, including precipitation, adsorption, nanofiltration, ultrafiltration, reverse osmosis, electrochemical technologies, and biological approaches have been applied to remove HMs from contaminated water bodies (Kumar et al. 2015).

Bioremediation approaches are competitive to conventional physical-chemical procedures as they are efficient, environmentally friendly and inexpensive (Chibueze et al. 2016). The application of microalgae in wastewater treatment (phycoremediation) has recently emerged as a promising solution because of its advantages over other bioremediation methods (Jais et al. 2017; Wollmann et al. 2019). Although several studies have documented the potential application of phycoremediation for the removal of Pb(II) from contaminated water. The majority of these studies have highlighted the application of inactive biomass of microalgae species as biosorbent without considering the application of growing cells (Flouty and Estephane 2012).

Despite the advantages of using growing cells over biosorbent biomass, only a few studies have described the potential application of live microalgae for the removal of Pb (II) from contaminated water (Liyanage et al. 2020; Pham et al. 2020; Piotrowska-Niczyporuk et al. 2015). It avoids the steps of cultivation, harvesting, drying, pre-treatment and conservation of biomass before it is used as a biosorbent (Malik 2004). Also, the use of growing cells of HMs-tolerant microalgae strains will further enhance the removal efficiency by the mean of both metabolism-independent (Biosorption) and metabolism-dependent (Bioaccumulation) mechanisms (Kumar et al. 2015). On the oher hand, under metal stress conditions, living microalgae produce various valuable substances such as polymers, proteins, pigments and lipids (Liu et al. 2016). Which offers a real opportunity to operate in a variety of industrial sectors, especially lipids, as a source of third-generation biofuels (Randrianarison and Ashraf 2017). Understanding the influence of HMs on the

biochemical composition of green microalgae is critical for a targeted valorization of the biomass and/or the metabolites produced during the phycoremediation process.

The aim of this study was to examine the mechanisms involved in Pb (II) phycoedimentation using live *S. obliquus*, and to investigate the changes in physicochemical properties, biochemical composition, and metabolomic profiling of the cells before and after Pb (II) phycoedimentation.

## Methods/experimental

### Strain and culture condition

The green alga *S. obliquus* used in this study has been previously selected as a Pb(II)-tolerant strain (Danouche et al. 2020). Its pure culture was sub-cultured at regular times in $BG_{11}$ medium (1.5 g $NaNO_3$, 40 mg $K_2HPO_4$, 36 mg $CaCl_2$ $2H_2O$, 6 mg ammonium citrate monohydrate, 6 mg ammonium ferric citrate, 1 mg ethylenediaminetetraacetic acid (EDTA), 2.86 mg $H_3BO_3$, 1.81 mg $MnCl_2$ $4H_2O$, 0.22 mg $ZnSO_4$ $7H_2O$, 0.39 mg $NaMoO_4$ $5H_2O$, 0.079 mg $CuSO_4$ $5H_2O$, 0.050 mg $CoCl_2$ $6H_2O$ in 1 L of distilled water) (Allen 1968). Experiments were performed with a pre-culture of *S. obliquus* obtained at the exponential phase. The biomass was firstly recovered by centrifugation at 4700 rpm for 10 min. Then, the pellet was diluted in Erlenmeyer flasks containing 100 mL of $BG_{11}$ medium for negative control and Pb(II)-doped medium at the concentration of $EC_{50}$ = 141 mg $L^{-1}$ corresponding to the half-maximal effective concentration (Danouche et al. 2020). The initial optical density (OD) of all experiments was adjusted to 0.350 ± 0.025 at $A_{680nm}$ using Ultrospec™ 3100 pro UV-Visible spectrophotometer, corresponding to 2 x $10^6$ cells $mL^{-1}$ equivalent. Flasks were incubated for 23 days under controlled conditions at 25 ± 2 ºC, under rotary shaking conditions at 150 rpm, and 10 h:14 h light-dark cycle.

### Growth inhibition, cells viability and size analysis

*Growth inhibition*: the growth kinetics of *S. obliquus* in control and Pb (II)-doped medium were monitored spectrophotometrically at two-day intervals. The linear relationship between

95 microalgal density (N, in cells per milliliter) and $OD_{680}$ was determined as reported by Zhou et al.
96 (2012) using CKX41 Olympus light microscope and a Malassez counting chamber with a depth of
97 0.2 mm. The calibration curve was as eq (1):

98 $$Y = 7.\ 10^6\ X + 2083\ (R^2 = 0.98) \quad \text{eq (1)}$$

99 Where Y is the number of cells (C $mL^{-1}$) and X denotes the OD at 680 nm. The specific growth
100 rate (SGR) (μ, in $day^{-1}$) was calculated in the exponential phase using eq (2), as described by
101 Aguilar-Ruiz et al. (2020).

102 $$\mu = \frac{\text{Ln X2} - \text{Ln X1}}{t2 - t1} \quad \text{eq (2)}$$

103 Where μ is the growth rate and $X_2$, $X_1$ represent the microalgal biomass concentration at $t_2$ and $t_1$
104 (time), respectively.

105 *Cells viability*: Pb(II) effect on the viability of *S. obliquus* was evaluated as described by da
106 Silva et al. (2009). An amount of $10^6$ cells from both control medium BG11 and Pb (II) doped
107 medium were centrifuged at 4700 rpm for 10 min, the pellet was then washed with phosphate buffer
108 solution (PBS, pH 7.0). Thus, the cells were exposed to 10 μg $mL^{-1}$ of propidium iodide (PI, Ref
109 81845 FLUKA) for 10 min in the dark and was directly analyzed by BD FACSCalibur Flow
110 Cytometry (FCM) System (BD Biosciences). PI is a fluorescent intercalating agent that intersperses
111 with double-stranded nucleic acids to produce red fluorescence when excited by blue light.
112 Undamaged membranes of microalgae are impermeable to PI, whereas, due to the loss in the
113 membrane integrity, the dye can input to the intracellular compartment (Suman et al. 2015). Heat-
114 inactivated cells were primed for positive control and processed under the same conditions. The
115 fluorescent emission of PI was collected from ~ 3000 events per sample. The PI was excited at 488
116 nm and measured at 585 nm ($FL_2$ channel) using the FACSCalibur optical system. Parameter
117 settings were adjusted to place the non-stained population in the negative area $FL_2/FL_1$ as an

autofluorescence control. Data were processed with CELLQuest Pro software (Becton Dickinson) and expressed as fluorescence arbitrary units. Cells viability was expressed as the percentage of cells viable versus the total number of cells acquired (Urrutia et al. 2019).

*Cells size analyses:* the size of *S. obliquus* cells grown in control medium and spiked with Pb (II) was measured by Malvern Zetasizer Zeta-Nano (England) working with laser doppler electrophoresis technique. The dynamic light scattering (DLS) method was used to determine changes in cell size after Pb(II)-phycoremediation (Xia et al. 2017).

### 2.3 Pb(II)-phycoremediation mechanism

Pb(II) uptake (biosorption and/or bioaccumulation) was first evaluated using thermogravimetric analysis (TGA Q500-Packaging-TA Instruments-USA) based on weight changes between control and Pb(II)-loaded biomass. In fact, under an inert nitrogen atmosphere, samples of equal weight were heated at a rate of 10 °C $min^{-1}$ up to 600 °C (Sudhakar and Premalatha, 2015). The TGA, as well as the difference thermogravimetry ratio (DTG) profiles of control and Pb(II)-loaded cells was plotted using excel software.

On the other hand, the discrimination between the intracellular biosorption and the extracellular bioaccumulation was carried out using chemical extractions as reported by Hassler et al. (2004), after Pb(II)-phycoremediation process, biomass was recovered by centrifugation (4700 rpm for 10 min). and the pellet samples were washed with EDTA solution ($5.10^{-3}$ M; pH 6.0). Dried samples of washed and unwashed biomass were then digested with 65% $HNO_3$ and 30% $H_2O_2$ in ACCblock digital dry bath (Labnet) for 40 min at 140 ºC. Pb(II) concentration in mineralized samples were measured using a Thermofisher 7000 series inductively coupled plasma optical emission spectrometer (ICP-AES). Thus, the Pb(II)-bioadsorbed onto the cells surface was determined by subtracting the intracellular Pb(II) concentration from the total Pb(II) removed.

For further insight into the Pb(II) bioremoval mechanism using living cells of *S. obliquus*, the intracellular concentration of $Na^+$, $K^+$, and their ratios were also analyzed. The decomposition of samples and the measurement of $Na^+$, $K^+$ concentration was performed as for the measurement of Pb(II) concentration

### 2.4 Physicochemical characterization of Cells-metal interaction

*Scanning electron microscope (SEM) coupled with Energy-dispersive X-ray spectroscopy (EDX):* SEM (JSM-IT500 InTouchScope™) was used to visualize the cells surface morphology of *S. obliquus* before and after Pb(II)-biosorption, while the EDX was employed to analyze the elemental composition from the imaged area. The analytical conditions were as follows: Signal SED, magnification of x1 000 - x55 000, landing voltage of 3.0 kV, work distance of 10.1 mm, at high vacuum mode.

*Fourier Transform InfraRed spectroscopy (FTIR):* in order to predict the functional groups on the cell wall of *S. obliquus.* Salt pellets were prepared using 1 mg of control and Pb(II)-loaded biomass and 149 mg of KBr, then compressed at 40 kN for 5 min. The pellets were analyzed using FTIR spectroscopy (ABB Bomem FTLA 2000 spectrometer analyzer). Thirty-two scans were performed at a range of 400 to 4000 $cm^{-1}$, with 4 $cm^{-1}$ of resolution for each sample.

*Zeta potential and Zero-point charge measurement:* in order to determine the zeta potentials of the biosorbents as a function of pH from 3 to 10. A volume of 100 mL of microalgae suspension was harvested by centrifugation (4700 rpm for 10 min), and then the pellet was resuspended in 10 mL of NaCl (0.1 M). The zeta potential was evaluated in the electrophoresis cell at 25 ºC using Nanosizer Nano (Malvern). For each pH value, triplicate measurements were taken, and approximately 30 readings were done for each data (Hadjoudja et al. 2010). The electrical state of the microalgae surface in solution was characterized using a zero-charge point (pHzc). Briefly, NaCl solutions (0.1 M) with pH ranging from 3 to 10 were prepared, then aliquots of 10 mL of

each pH-adjusted NaCl solution were mixed with 50 mg of the biomass, shaken for 24 h at 25 ºC, and the final pH values were measured. The difference in ΔpH was plotted against the initial $pH_i$ to determine the pHzc (Zehra et al. 2016).

*Contact angle measurements*: the contact angle measurement of control and Pb(II)-loaded cells was performed at 25 ºC as described by Asri et al. (2018), using a digital optical contact angle (Data Physics OCA 40), via the sessile drop method, using water, formamide, and diiodomethane (Table 1). Both the left and the right contact angle measurements of both biomasses were automatically calculated from the digitalized image using SCA 20 software for OCA and PCA operated under Windows 7. Degree of hydrophobicity of control and Pb(II)-loaded cells were then estimated according to Vogler's and Van Oss approach (Van Oss et al. 1988; Vogler, 1998).

**Effect of Pb(II) on the biochemical composition**

*Photosynthetic pigments analysis:* impact of Pb(II) ions on the photosynthetic system was firstly evaluated based on the autofluorescence using the FCM system. When cells are excited by red (635 nm) and blue (488 nm) diode lasers, the chlorophyll can be observed in both orange ($FL_2$: 585/42 nm) and red ($FL_3$: 530/30 nm) fluorescence emission. The phycoerythrin is excited with the argon laser (488 nm) and emits in the orange region, the fluorescence can be measured at the $FL_2$ channel. Regarding the phycocyanin, it's generally excited with diode laser and emits at the $FL_4$ (661/16 nm) channel. On the other hand, the pigment content was also assayed spectrophotometrically using the method of Tahira et al. (2019). Pigment extraction from biomass collected from both mediums was prepared at a concentration of 1 mg $mL^{-1}$ in 95% ethanol. Biomass were then homogenized by a SONOPULSmini20 ultrasonic homogenizer at 4 ºC and kept overnight in the dark at 4 ºC. Thus, the homogenate was centrifuged for 10 min at 4700 rpm. Finally, the absorbance of both samples was measured spectrophotometrically at 470 nm, 649 nm,

and 664 nm. The pigments contents of chlorophyll a (Ch-a), chlorophyll b (Ch-b), and the total carotenoids (C $x_+c$) was calculated based on Lichtenthaler and Buschmann (2001) equations:

- ✓ Ch-a =13.36 $A_{664}$ - 5.19 $A_{649}$ eq (3)
- ✓ Ch-b =27.43 $A_{649}$ - 8.12 $A_{664}$ eq (4)
- ✓ C $x_+c$ = (1000 $A_{470}$ - 2.13 Ch-a - 97.63 Ch-b) / 209 eq (5)

*Proteins, lipids, and carbohydrates determination*: the extraction of total lipid were achieved with a solvent mixture: water: chloroform: methanol (1:2:1) as reported by El Arroussi et al. (2017). The biomass mixture (1 mg $mL^{-1}$) was centrifuged for 5 min at 4700 rpm, the chloroform layer was recovered and evaporated using nitrogen gas, and the total lipids were weighed. The estimation of neutral and polar lipid content in cells of *S. obliquus* from control and Pb(II)-doped medium was also evaluated employing the multi-parameter FCM with the fluorescent stain Nile Red (NR) as reported by da Silva et al. (2009). Lipids' straining with NR is traduced to different fluorescence emissions after excitation with the argon laser at 488 nm. When NR is dissolved in neutral lipids it emits an intense yellow fluorescence collected in the $FL_2$ channel, and when dissolved in polar lipids it exhibits red fluorescence collected in the $FL_3$ channel (Jara et al. 2003). For the protein's extraction, 50 mg of lyophilized microalgal biomass was homogenized using the ultrasonic homogenizer (Sonopuls mini20) in the ice bath assisted by freezing cycles thawing at -80 ºC. The homogenate was next centrifuged at 4700 rpm for 15 min at 4 ºC. The supernatant was used for the estimation of the total soluble proteins using the Bradford method and bovine serum albumin (BSA) as standard (Bradford 1976). Total soluble sugars were estimated using the protocol described by Wychen and Laurens (2017). The biomass was hydrolyzed by two-step sulfuric acid hydrolysis first in 72% (w/w) sulfuric acid for 1 h at 30 ºC. Then place in an autoclave for 1 h at 121 ºC with 4% (w/w) sulfuric acid. Finally, the total soluble carbohydrate content was assessed via the phenol-sulfuric acid colorimetric method (Dubois et al. 1956).

**Metabolomics profiling of control and Pb(II)-loaded cells**

Metabolomics profiling of *S. obliquus* cultivated in control and Pb(II)-doped medium were analyzed using a Gas chromatography-mass spectrometry (GC-MS) (Agilent 7890A Series GC). Firstly, 50 mg of both biomasses were recovered by centrifugation. Thus, the pellets were washed with sterile distilled water and transferred in 15 mL conical centrifuge tubes prepared in a dewar filled with liquid nitrogen. Non-polar metabolites were secondly extracted using a solvent mixture: water: chloroform: methanol (1:2:1) (El Arroussi et al. 2017).

*Non-polar metabolites determination using transesterification reaction:* the transesterification reaction was performed using 6% $H_2SO_4$-methanol at 80 ºC, and atmospheric pressure during 3 h, assisted by ultrasonication in Branson ultrasonic (Soniffier 450) bath at 40 kHz as described by Mutale-joan et al. (2020). 2 mL aliquots of chloroform-solubilized metabolites were analyzed by GC using split mode (1:4) with the helium at 1.5 mL $min^{-1}$ as carrier gas. The ion source and quadruple temperatures were 230 ºC and 150 ºC respectively. The oven temperature program started at 30 ºC, then it was increased by 10 ºC $min^{-1}$ to 120 ºC, increased until 200 ºC by 30 ºC $min^{-1}$, increased to 250 ºC by 10 ºC $min^{-1}$, temperature and hold for 1 min at the end of each phase. Finally, the temperature was increased to 270 ºC by 5 ºC $min^{-1}$ and kept constant for 5 min. The detection was achieved by full scan mode between 30 and 1000 m/z, with a gain factor of 5 (El Arroussi et al. 2015).

*Metabolite identification, data mining, normalization, and statistical analysis:* metabolites detected by GC-MS were identified with MS NIST 2014 library, as having predictability greater than 90%. The classification of these metabolites was carried out by PubChem® and LIPID MAPS® structure database. To correct heteroscedasticity and pseudo-scaling, the power transformation was carried out on the obtained data (van den Berg et al. 2006). The quantities of individual fatty acids were calculated from the peak areas using dodecane as an internal standard.

236 **Statistical analysis**

237 Experiments were carried out in triplicate, and data were expressed as the mean ± standard
238 deviation. The statistical analysis of the differences between cells of *S. obliquus* from control and
239 Pb(II)-doped medium was performed with unpaired T-test, and two-way ANOVA by Sidak's
240 multiple comparisons test using GraphPad Prism software version 8.0. The P-values of $< 0.05$ were
241 considered to be statistically significant. The heat map generation was performed using RStudio,
242 and the visualization by FactoMineR package, integrated into the R software.

243 **Results and discussion**

244 ***S. obliquus* growth inhibition, cells viability and size**

245 The kinetic of growth and the SGR of *S. obliquus* cultured in control and Pb(II)-doped
246 medium are illustrated in Fig. 1A. Growth inhibition was monitored throughout the exponential
247 phase to determine the effect of Pb(II) ions on growth and to distinguish it from growth inhibition
248 caused by nutritional deficiency. During the first week of culture, the growth kinetics of *S. obliquus*
249 in Pb(II)-doped medium showed no significant inhibition compared with control cells. However,
250 from 7th day of culture, significant growth inhibition was observed and continued until the
251 beginning of the stationary phase. As shown in Fig 1B, the SGR of *S. obliquus* in both media
252 decreased considerably during the first week. Though, from the 13th day of culture, it was
253 maintained at a stationary level. This finding is consistent with previous research reporting the
254 inhibitory effect of Pb(II) ions against *Chlamydomonas reinhardtii* (Li et al. 2021).

255 As depicted in the cytogram (Fig. 1C), the viability of the negative control (cells from control
256 medium) was at 96.07%. However, the rate of living cells versus the negative control was decreased
257 by 6.3% after exposure to Pb(II) ions. The viability of heat-inactivated cells used as a positive
258 control was 0.07%. From the obtained results, we can conclude that the Pb(II) at the $EC_{50}$
259 concentration of 141 mg $L^{-1}$ has a low effect on the integrity of cell membrane. To our knowledge,

there is a few research that has focused on assessing cells viability after HMs-phycoremediation using FCM system. For example, Nazari et al. (2018) reported a significant decrease in viability of *C. vulgaris* treated with reduced graphene-silver oxide nanocomposites. A similar effect was also observed in *C. vulgaris* exposed to zinc oxide nanoparticles (Suman et al. 2015).

Pb(II) ion induced a slight decrease in cell diameter and cell volume of *S. obliquus* at EC50 concentration (Fig. 1D). This change can be attributed to the decrease of cells density, compensated by the decrease of cells biovolume. In line with this finding, Kim et al. (2016) indicated a reduction in the biovolume of *Chlorella* cells exposed to a high dosage of magnesium aminoclay (MgAC) compared to the control cells. Conversely, Romero et al. (2020) reported that the diameter and the volume of *C. vulgaris* had been enhanced following exposure to silver nanoparticles (AgNPs). It is noteworthy that biovolume is an important parameter in studies of microalgal population dynamics, phytoplankton physiology, ecosystem energy, etc. However, this parameter is not commonly considered in ecotoxicological research (Thomas et al. 2018).

**Pb(II)-phycoremediation mechanism**

As illustrated in Fig 2A, the TGA and DTG profiles of control and Pb(II)-loaded biomass have indicated that there are three phases of decomposition of *S .obliquus* biomass. The first stage (from 25 to 250 ºC), corresponding to the weight losing process of volatile compounds, the second stage (from 250 to 445 ºC) belongs to the devolatilization process, and the third stage (more than 445 ºC) consistent with the slow decomposition of the inorganic residue of ash. In agreement with these findings, Marcilla et al. (2009) noted that the TGA and the DTG of the thermal pyrolysis of *Nannochloropsis* sp., have also three main decomposition steps (<180 ºC, 180 - 540 ºC, and > 540 ºC). It is clearly illustrated in Fig. 2A that the rate of residue weight of cells after Pb(II)-biosorption (57.8%) was higher than that of cells from the control medium (31.34%). Moreover, the DTG showed that the weight loss at 315 ºC was 0.588% for control biomass and 0.346% for Pb(II)-

loaded cells. This difference in weight loss would be related to the composition of the cells after Pb(II) biosorption and/or bioaccumulation. According to Chinedu et al. (2012), the difference in the weight can be related to the inorganic content of the ash biomass from the contaminated medium. Moreover,. Venkata Mohan et al. (2007) showed that the heat required for thermal degradation of *Spirogyra* sp. was higher after biosorption of fluoride, compared to the control cells, which could be the result of the ionic bond formed after biosorption.

Regarding the discrimination between extracellular biosorption and intracellular bioaccumulation, the concentration of Pb(II) in washed and unwashed cells ranged from 9.2 mg $L^{-1}$ and 54.2 mg $L^{-1}$, respectively (Fig. 2B). This result indicates that both bioaccumulation (14.5%) and biosorption (85.5%) mechanisms are implicated in the phycoremediation of Pb(II). There are only a few types of research that have focused on the discrimination between bioaccumulation and biosorption, it has been reported that the phycoremediation of Cd(II) by living *Tetraselmis suecica* involves both mechanisms, intracellular bioaccumulation and extracellular biosorption (Pérez-Rama et al. 2002).

The analysis of the concentration of $Na^+$, $K^+$ and their ratios in cells of *S. obliquus* from control and Pb(II)-dopped medium, the findings illustrated in the Fig. 2C indicate a significant decrease in the concentration of $Na^+$ ions in Pb(II)-loaded cells, compared to control cells. However, no significant change was noticed in the concentration of the $K^+$ ions. It has been reported that $Na^+$ can play several functions in the process of phycoremediation. The cell surface of microalgae incorporates many ions ($K^+$, $Ca^{2+}$, and $Mg^{2+}$) of which $Na^+$ constitutes the major part; such ions can be reversibly replaced by other toxic ions via a process called ion exchange (Navakoudis and Ververidis 2018). On the other hand, we can also hypothesize that Pb(II) bioaccumulation can be managed by the flow of $Na^+$ ions to establish cellular homeostasis. These results are in agreement with the results of the cells size. The maintenance of cells size is related

to the regulation of sodium pumps, which is accomplished through the pump-leak mechanism (Kay 2017).

**Physicochemical characterization of Cells-metal interaction**

Characterization of the cell morphology and elemental composition of the *S. obliquus* surface (control and Pb(II)-loaded cells) was first performed using SEM and EDX analyses. Fig. 3A and B display respectively the SEM images of *S. obliquus* before and after Pb(II)-biosorption at 8000× magnification. Notable differences in cells appearance were observed in Pb(II)-loaded cells compared to control cells. Indeed, a white appearance appears on the cells after Pb(II) biosorption, which reflects the absorption of Pb(II) ions by the cell walls. The analysis with the X-ray confirmed also these observations, as shown in Fig. 3C, the presence of X-ray peaks representing C, P, O, S, K, Mg, Ca and Si, before Pb(II)-biosorption are attributed to the components of the cell wall. While a notable change was observed in the elemental composition after Pb(II)-biosorption, with disappearance of the peaks corresponding to Si and S in the 2.2 - 2.3 KeV region, and this peak was replaced by a peak corresponding to Pb. As showed in the Fig. 3D, there was a variation in the intensity level of the other detected elements. There were two regions of peaks related to Pb in Pb(II)-loaded cells, the first one was on the low-energy region (2.2 KeV) and five other peaks were detected on a second high-energy region of the EDX spectrum, thereby confirming the variation of the distribution of Pb uptake by *S. obliquus.* It can be attributed to its intracellular accumulation, which occurs in two successive steps: an initial rapid, passive and non-specific uptake of HMs ions onto the cell wall. Followed by an active and/or passive transport across the cell wall and plasma membrane to the cytoplasm (Kumar et al. 2015). According to Pérez-Rama et al. (2002), the Cd(II)-uptake using *Tetraselmis suecica* was a biphasic process, assisted in the first phase by an adsorption to proteins or polysaccharides, followed by an energy-dependent accumulation to the cytosol. This finding is agreeing with the results of ICP and TGA analyses.

The FTIR spectra (Fig. 3E) of *S. obliquus* revealed a heterogeneity composition of the cell wall, evidenced by different peaks characteristic of lipids, proteins, and carbohydrates. Significant changes in the functional groups of the cell wall were demonstrated after biosorption of Pb(II) ions. The absorption peaks at the region between 3200 and 3600 $cm^{-1}$ indicated the existence of stretching vibration of hydroxyl (-OH) and amino ($-NH_2$) groups, which are among the functional groupings of chitosan and amino acids. The peaks around the region 3000 - 2800 $cm^{-1}$ showed the stretching vibration functional of Methyl, and Methylene groups ($-CH_3$, $-CH_2-$). The peaks at 1650 and 1542 $cm^{-1}$ would be caused by the bending and stretching of amine ($-R_2-NH$) groups of the proteins. The peaks around 1400 and 1200 $cm^{-1}$ may be caused by sulfur group (-SO-), and phosphorous group (-PO-) that compose the phospholipid membrane. The peaks at 1026 $cm^{-1}$ elongation of bonds C-C, C-O, and C-N, correspond to the polysaccharides (He and Chen 2014). After Pb(II)-biosorption, a significant decrease in the transmittance of the surface peaks was recorded, which may be attributed to its occupation by Pb(II) ions. Furthermore, the comparison of FTIR spectra of *S. obliquus* biomass before and after Pb(II) biosorption showed a shift in functional groups of cells loaded to Pb(II) ions. The main shifts were detected in the absorption bands of hydroxyl, carboxylic acid, amine and amino groups. These functional groups have been previously identified on the cell wall of various microalgae species (Zheng et al. 2016). The outcome suggests that Pb(II)-biosorption involves π-cation interactions between the cells surface and cations in the solution (Tran et al. 2017). Furthermore, some previous studies also indicated that biosorption process was accomplished by chelation and formation of ionic bridges between HMs and functional groups (Jena et al. 2015).

The electrical state of the cells surface is also one of the critical parameters in biosorption studies. Thus, the measurement of zeta potential, as well as the pHzc of *S. obliquus* cells are among the keys parameters related to the external loads of the adsorbent (Akar et al. 2009). As shown in

Fig. 3F, the zeta potential of *S. obliquus* was maintained at a negative charge, regardless the initial pH value. Indeed, it varied from -8.17 mV at pH 3 to -36.13 at pH 6.5. This result testifies the anionic characteristics and the high concentration of acid functional groups on the cell wall surface. Furthermore, at pHi, the zeta potentials of control cells were more negatively charged (-36.13 mV) than the Pb(II)-loaded microalgae cells (-32.5 mV) (Fig. 3F and G). The value of pHz at which the $\Delta pH = 0$ was at 6.45 (Fig. 3H), confirming the dominance of anion groups over cation groups on the cells surface. These negatively charged groups permit the binding of ions from the surrounding environment, making the outer layer of the cell wall as the first participator in the removal of HMs (Leong and Chang 2020; Saavedra et al. 2018; Singh et al. 2021). These findings are consistent with previous research that evaluated the zeta potential of different microalgae strains. For instance, Li et al. (2017) had shown that the zeta potential was charged negatively at all growth phases of *Desmodesmus bijugatus*, *Botryococcus* sp and *Chlorella* sp. Also, Samadani et al. (2018) reported that the average of the zeta potential of *Chlamydomonas* was at - 41 mV, - 4mV respectively at pH 7 and pH 4, they propose that at low pH, the zeta potential around to the zero can reduces the electrostatic interactions between the metal cations and the cell wall surface, thereby reducing the cationic fluxes into the cells.

Based on both Vogler's and Van Oss approaches, *S. obliquus* exhibited a hydrophilic character, the $\theta_w$ value (34.9° ± 0.4) was less than 65° (Table 2), and the ΔGiwi had a positive value (37.23 ± 1.13 mJ $m^{-2}$). These findings agree with previous results reporting the hydrophilic character of various microalgae strains (Ozkan and Berberoglu 2013). It has been reported that cell surface hydrophobicity is related to the presence of proteins in the cell wall (Vichi et al. 2010). Additionally, cells of *S. obliquus* appear to behave predominantly as electron donors/Lewis bases with high values of $\gamma^- = 52.57 \pm 0.6$ mJ $m^{-2}$. These results indicate that this strain exhibit a weak electron acceptor character with $\gamma^+ = 0.24 \pm 0.07$ mJ $m^{-2}$. Previous studies have also demonstrated

the electron donor character of several microorganisms, which has been correlated with the presence of various phosphate groups in the cell wall (Vichi et al. 2010). These finding are consistent with the FTIR analyses that confirm the presence of phosphate groups on its cells surface. On the other hand, after Pb(II) biosorption, the $\theta_w$ of *S. obliquus* significantly decreased from 34.9° ± 0.4 to 31.6° ± 0.9 (Table 2). This can be explained by an increase in the density of polar functional groups on cell surfaces after Pb(II) biosorption (Yalçin et al. 2010). Additionally, a significant variation was noted in the electron donor and acceptor character after Pb(II)-biosorption ($\gamma^+$ from 0.24 ± 0.07 to 0.08 ± 0.02 mJ $m^{-2}$; and $\gamma^-$ from 52.57 ± 0.6 to 59.79 ± 0.5 mJ $m^{-2}$) due to the interaction of functional groups in the cells surface with the Pb(II) ions.

**Pb (II) influence on the biochemical composition of *S. obliquus***

*Effect of Pb(II) on the photosynthetic pigments:* cells of green microalgae are autofluorescent, their signature can be observed in the red, orange and green channel using FCM system. As shown in Fig. 4, Pb(II) cause an alteration in the autofluorescence of *S. obliquus* pigments. Indeed, a shift in autofluorescence of native pigments of Pb(II)-loaded cells (B, D, F, and H) was observed in comparison with cells from the control medium (A, C, E, and G). The orange fluorescence is much lower than the chlorophyll autofluorescence, as detected in the red channel. It has been reported that the intensity of orange, green and red autofluorescence vary in response to changes in the physiological state of the algae due to oxidative stress (Ying and Dobbs 2007). In line with our finding, Cheloni and Slaveykova (2013) also reported a change in the autofluorescence of *C. reinhardtii* exposed to metallic (copper, mercury, and nanoparticulate copper oxide). Subsequently, spectrophotometric measurement of pigment content showed a significant decrease in the concentration of Ch-a and Chl-b in *S. obliquus* cells grown in Pb(II)-doped medium compared to cells in control medium (Fig. 4I). The total Chl-a and Chl-b were reduced from 54.08% to 52.5% and from 30.99% to 20.1%, respectively. In contrast, total C x+c increased from 14.93% to 27.3%

404 in Pb(II)-loaded cells. In keeping with this finding, Piotrowska-Niczyporuk et al. (2015) has
405 reported that the total C x+c in *Acutodesmus obliquus* was less influenced by Pb(II) ions as
406 compared to the chlorophyll pigments. According to Nazari et al. (2018), the decrease in
407 chlorophyll content is one of the main indicators of oxidative stress in microalgae. The reduction
408 in chlorophyll content can be explained by the inhibition of their biosynthesis, by an eventual
409 degradation, or by the alteration of the thylakoid system as a consequence of the binding of metals
410 to proteins, perturbing therefore its normal function (Carfagna et al. 2013; Piotrowska-Niczyporuk
411 et al. 2015). Regarding the increase of C x+c levels in Pb(II)-loaded cells, it has been reported that
412 shuch class of pigments provides protection to photosynthetic membranes against reactive oxygen
413 species (Piotrowska-Niczyporuk et al. 2015; Rai et al. 2013).

414 *Effect of Pb(II) on the content of proteins, lipids, and carbohydrates:* biochemical
415 characterization of S. obliquus biomasses revealed that Pb(II) stimulates lipid production, a
416 significant increase from 14.58% in control cells to 22.14% in Pb(II)-loaded cells was observed.
417 Several previous studies confirm this statement, As a recent example, the study of Nanda et al.
418 (2021) that showed an increase in lipid content in *Chlorella sorokiniana* grown under Pb(II) stress.
419 Also, Napan et al. (2015)reported an increase in lipid yield in *S. obliquus* grown in the presence of
420 different metals (As, Cd, Co, Cr, Cu, Hg, Ni, Pb, Se and Zn). Similarly, Han et al. (2019) showed
421 that lipid productivity in *S. obliquus* was significantly increased by 27.95%, 19.21% and 18.63%
422 respectively after supplementation with trace metals of Fe, Mn, and Mo. In contrast, Pham et al.
423 (2020) found that Pb(II) concentration around 0.5 and 1 mg $L^{-1}$, significantly increased the
424 production of the total lipids content, but the increase in Pb(II) concentration to 10 mg $L^{-1}$ shows a
425 reverse effect. With regard to the neutral and polar lipids, it were examined with the FCM system.
426 As shown in the cytograms (Fig. 4K and L), the signal collected in the $FL_2$ channel is stronger for
427 Pb(II)-loaded cells compared to cells from the control medium, which means that an increase in

neutral lipid fluorescence occurred in the stressed cells compared to the control. under several stress conditions, microalgae accumulate lipid bodies as energy reserves. Moreover, neutral lipids are part of the essential components of membranes such as glycol and phospholipids (Benhima et al. 2018). In the present research, the increase in natural lipid content in Pb(II)-loaded cells could be an adaptive mechanism against oxidative stress caused by Pb(II) ions.

In contrast, the carbohydrate and protein content shows a significant decrease in Pb(II)-loaded cells. It was from 14.35% to 10.6%. and from 15.68% to 11.6% for the content of carbohydrates and proteins, respectively. These findings are in agreement with previous study. It has been reported by Belghith et al. (2016) that soluble and insoluble carbohydrates in *Dunaliella salina* biomass decreased significantly with increasing Cd(II) concentration. However, Tahira et al. (2019) noticed an increase in total sugar content in *Euglena gracilis* in response to As(III) ions. Moreover, Piotrowska-Niczyporuk et al. (2015) noticed a gradual decrease in the contents of soluble and insoluble proteins of *A. obliquus* exposed to Pb(II) ions. According to Dittami et al. (2009), genes involved in primary metabolism and protein synthesis are downregulated, while genes related to autophagy and protein degradation are activated under stressed conditions. In the context of biorefineries, the results of the present study are very promising since the selected strain can accumulate lipids after Pb(II)-phycoremediation. Therefore, it is possible to use such lipids for the production of third generation biofuels or for other types of applications.

**Metabolomics profiling of control and Pb(II)-loaded cells**

In this section, the metabolomic profiling of (i) fatty acids, (ii) alkanes and alkenes, (iii) sterols and other compounds detected in *S. obliquus* cells grown in control, and Pb(II)-doped medium was analyzed. Fig. 5 summarizes the metabolite profile of control (A) and Pb(II)-loaded cells of *S. obliquus* (B). Indeed, a total of 54 and 59 putative compounds were detected respectively in the resulting biomasses. Compared to control cells, Pb(II)-loaded cells showed a significant

increase in the relative abundance of fatty acid methyl esters (FAME) (15% to 18%), Alkanes (3% to 8%), aromatic compounds (2% to 13%) and sterols (1% to 2%). However, the amount of monounsaturated fatty acids (MUFA) was decreased from 22% in control to 5% in Pb(II)-loaded cells. Also, alkenes were reduced from 3% to 2%. Regarding the amount of saturated fatty acids (SFA), no clear variations were noted, and the polyunsaturated fatty acids (PUFA) were only detected in the control biomass. Previous metabolomic studies on microalgae have mainly focused on the identification and valorization of algal metabolites in the agri-food (polysaccharides, fatty acids...), pharmaceutical (carotenoids, steroids...), and public health (algal toxins) fields (Richmond, 2004). A very limited number of research studies have been focused on the metabolomics analysis of microalgae after phycoremediation of HMs.

*Fatty acid composition:* Among the primary parameters to be studied in lipidomic research are the composition and degree of saturation of fatty acids. As shown in Fig. 5C. The composition and concentration of fatty acids identified in cells from control and Pb(II)-doped medium were significantly different. A set of 28 fatty acids was detected, which belong to 4 subclasses including SFA (12), MUFA (7), PUFA (1), and FAME (8). The most abundant SFAs in both biomasses are palmitic acid ($C_{16:0}$), pentadecanoic acid ($C_{15:0}$) and stearic acid ($C_{18:0}$). However, Pelargonic acid ($C_{9:0}$) and Cerotic acid ($C_{26:0}$) were present only in the control cells. Nevertheless, the Myristic acid ($C_{14:0}$) and Margaric acid ($C_{17:0}$) were detected only in the Pb(II)-loaded cells. The concentrations of Lauric acid ($C_{12:0}$), Pentadecanoic acid ($C_{15:0}$), Stearic acid ($C_{18:0}$), Lignoceric acid ($C_{24:0}$), and Montanic acid ($C_{28:0}$) were higher in the control cells compared to Pb(II)-loaded cells. Conversely, the concentration of Palmitic acid ($C_{16:0}$) was higher in Pb(II)-loaded cells. The concentrations of Behenic acid ($C_{22:0}$) and Melissic acid ($C_{30:0}$) were almost equal in both biomasses. Except for oleic acid ($C_{18:1\omega 9}$), all MUFAs were found only in control cells. As regards the PUFA, linoleic acid ($C_{18:2:9.12}$) was detected only in the control cells. The following FAME: Methyl tetradecanoate

476 ($C_{15}H_{30}O_2$), Methyl 13-methyltetradecanoate ($C_{16}H_{32}O_2$), and Methyl octadecanoate ($C_{19}H_{38}O_2$)
477 were present in both biomasses. Whereas, Methyl 20-methyl-heneicosanoate ($C_{23}H_{46}O_2$), Methyl
478 11-(3-pentyl-2-oxiranyl) undecanoate ($C_{19}H_{36}O_3$), Methyl 2-hydroxy-tetracosanoate ($C_{25}H_{50}O_3$),
479 and Methyl 5,9-hexadecadienoate ($C_{17}H_{30}O_2$) were detected only in Pb(II)-loaded cells.
480 Oppositely, Methyl 2-octylcyclopropene-1-heptanoate ($C_{19}H_{34}O_2$) was detected in the control cells.
481 To our knowledge, no previous study has examined the effect of Pb(II) ions on the metabolic
482 profiling of *S. obliquus* following the phycoremediation process. Only a few studies have been
483 conducted on the lipidomic profiling of some microalgae strains exposed to HMs. The results of
484 the present study indicate that a number of changes can occur in the overall lipids content, and their
485 degree of saturation. Among all lipid classes, fatty acids (FAs) are the most abundant in microalgae,
486 as well as they are generally the most influenced by metal stress (Guschina and Harwood, 2006).
487 Consistent with the result obtained, similar observations have also been reported in the literature
488 regarding the influence of HMs on the lipidomic profile of certain microalgal strains (Rocchetta et
489 al. 2012, 2006; Sibi et al. 2014). For instance, the lipid profiles of *C. sorokiniana* under Pb(II)
490 stress increased the levels of $C_{14}$, $C_{16}$, and $C_{18:1}$. However, the levels of $C_{16:1}$, $C_{18}$, $C_{18:2}$, $C_{18:3}$, and
491 $C_{20}$ were reduced as compared to control cells (Nanda et al. 2021). It has been also reported that
492 the FAs can play several roles in various physiological functions, like a bioindicator of the
493 adaptation of the cell membranes to the environmental conditions (Filimonova et al. 2016).
494 Moreover, under stress conditions, cells of microalgae stimulate the synthesize and the
495 accumulation of energy reserves, mainly in the form of TAG (Minhas et al. 2016). It is known that
496 PUFAs are the lipid fraction involved in the maintenance of structural functions. Whereas, SFA
497 and MUFA constitute among others the energy reserves (Olofsson et al. 2012). These findings can
498 be explained by the biochemical adaptation mechanism. Indeed, under metal stress conditions, cells
499 of microalgae change their metabolism via an adjustment of the ratio between unsaturated and

saturated fatty acids, in order to reduce the permeability and or fluidity of the cell membrane prevent therefore the intracellular bioaccumulation of HMs ions across the cell membrane (Lu et al. 2012).

*Alkanes and Alkenes*: As illustrated in Fig. 5D, a large variation in alkane and alkene composition was evident in cells grown in control versus Pb(II)-doped medium. The relative abundance of saturated hydrocarbons (alkane) was higher than unsaturated hydrocarbons (alkenes). The diversity of saturated hydrocarbons showed that the content of n-alkanes ranging from n-$C_{17}$ to n-$C_{36}$, and they are dominated by very long chain alkanes. A total of 15 alkane metabolites were detected in Pb(II)-loaded cells, compared with 11 in control cells. The long-chain (L.C) alkanes are present in both biomasses, the content of n-$C_{17}$, n-$C_{18}$, and n-$C_{20}$ decrease slightly in Pb(II)-loaded cells. However, a remarkable increase was recorded for n-$C_{21}$ and n-$C_{22}$. The distribution patterns of very-long-chain alkanes (V.L.C) varied from 10 in Pb(II)-loaded cells to 6 in control cells. One branched long-chain alkanes (2-Methyltriacontane ($C_{31}H_{64}$)) was at an equal amount in both biomasses. Though four V.L.C alkanes: Hexacosane ($C_{26}H_{54}$), Heptacosane ($C_{27}H_{56}$), Pentatriacontane ($C_{35}H_{72}$), and Hexatriacontane ($C_{36}H_{74}$) have been detected only in Pb(II)-loaded cells. Regarding the analysis of the alkene profile, 8 alkenes were detected, they are distributed as follows: in the cells from the control medium, four L.C and one V.L.C alkenes, while, two L.C, and two V.L.C alkene was detected in Pb(II)-loaded cells. The analysis of alkene data showed that the position of the double bond "C=C", in the alkene from cells grown in the control medium, was located in the first position (1-Heptadecene, 1-Octadecene, 1-Eicosene, 1-Heptacosene), while a change in this position to 9 and 10 (10-Heneicosene ($C_{21}H_{42}$), 9-Tricosene ($C_{23}H_{46}$) and 9-Hexacosene ($C_{26}H_{52}$)) in Pb(II)-loaded cells. In the available literature, no previous studies have been investigated the effect of Pb(II) ions on the alkane and alkene profiles of green microalgae. It has been reported that hydrocarbons can play several roles in microalgal cells. Due to their high

hydrophobicity, they contribute to the regulation of the fluidity of photosynthetic membranes and also act in intercellular signaling (Sorigué et al. 2016). It is evident that additional omics research is needed to identify the biochemical pathways responsible for the synthesis of alkanes and long-chain alkenes in microalgal cells under metal ion stress conditions, in order to identify the mechanisms by which they are involved in managing such oxidative stress.

*Sterol and aromatics:* After lipids transesterification, sterol and some aromatic compounds were also identified in the organic phase. Two sterols were detected in *S. obliquus* cells from control, and Pb(II)-doped medium: (20.Xi.-Lanosta-7,9(11)-diene-3.b...) and (Lanost-8-en-7-one). However, (9,19-Cyclocholest-24-en-3-ol) was detected only in control cells, and (Cholestan-3-ol) was detected only in Pb(II)-loaded cells. On the other hand, 11 aromatic molecules were detected in Pb(II)-loaded cells, and 3 in control cells (data not shown). The common feature of aromatic compounds detected in Pb(II)-loaded cells is the presence of radical ketone groups such as 2H-pyrrol-2-one, 2H-Inden-2-one, 2(3H)-Furanone, and 2H-pyrrol-2-one. Sterols are usually good chemotaxonomic tools for studying microalgal biochemistry. In contrast to fatty acid compositions, the differences in the relative proportions of sterols with varying environmental conditions were minorly investigated (Volkman 2016). The published literature on sterol composition of microalgae continues to grow, however, is still far from complete in terms of implications for resistance to possible oxidative stress generated by HMs.

## Conclusions

Based on the above considerations, we can deduce that phycoremediation of Pb(II) ions using living cells of *S. obliquus* involves both extracellular biosorption and intracellular bioaccumulation. The physicochemical characterization of control and Pb(II)-loaded cells using a range of physicochemical characterization analyses (SEM-EDX, FTIR, zeta potential, zero-point charge, and contact angle measurements) has confirmed the involvement of several chemical and

electrostatic interactions between the macromolecules constituting the cell surface and the Pb(II) ions in solution. The comparison of the biochemical and metabolomic profile of *S. obliquus* grown in control and Pb(II)-doped medium revealed that cells subjected to Pb(II) exposure conditions adjust their metabolism, particularly lipid biosynthesis, in order to reduce the permeability and fluidity of cell membranes, preventing therefore the intracellular accumulation of Pb(II) ions that might cause a variety of damage.

**Abbreviations**

Optical density (OD); specific growth rate (SGR); phosphate buffer solution (PBS); Propidium iodide (PI); BD FACSCalibur Flow Cytometry (FCM); Dynamic light scattering (DLS); Thermogravimetric analysis (TGA); Thermogravimetry ratio (DTG); Inductively coupled plasma atomic emission spectroscopy (ICP-AES); Scanning electron microscope (SEM); Energy-dispersive X-ray spectroscopy (EDX); Fourier Transform InfraRed spectroscopy (FTIR); Zero-charge point (pHzc); Lifshitz–van der Waals ($\Upsilon^{LW}$); electron-donor ($\Upsilon^{-}$); and electron-acceptor ($\Upsilon^{+}$); surface energies ($\Delta Giwi$); Nile Red (NR); Bovine serum albumin (BSA); Gas chromatography-mass spectrometry (GC-MS); Fatty acid methyl ester (FAME); Monounsaturated fatty acids (MUFA); Saturated fatty acids (SFA); Polyunsaturated fatty acids (PUFA); Aromatic compounds (Arom.); Very long-chain alkanes (V.L.C); Long-chain alkanes (L.C).

**Acknowledgements**

The authors gratefully acknowledge the Moroccan Foundation for Advanced Science, Innovation and Research (MAScIR), and Regional University Centre of Interface (CURI), Sidi Mohamed Ben Abdellah University for their financial and technical support.

**Authors' contributions**

**M. Danouche**: Conceptualization, Methodology, Formal analysis, Writing - original draft, Visualization. **N. El Ghachtouli**: Supervision, Writing - review & editing. **Aasfar A**. Formal

572 analysis, **Bennis I**. Formal analysis. **H. El Arroussi**: Supervision, Conceptualization, Writing -
573 review & editing, Validation, Resources, Funding acquisition, Project leading

574 **Funding**

575 Not applicable.

576 **Availability of data and materials**

577 The data sets used and/or analyzed during the current study are available from the corresponding
578 author on reasonable request.

579 **Declarations**

580 **Ethics approval and consent to participate**

581 Not applicable.

582 **Consent for publication**

583 Not applicable.

584 **Competing interests**

585 The authors declare that they have no competing interests

586 **References**

587 Aguilar-Ruiz R J., Martínez-Macias M del R, Sánchez-Machado D I, et al (2020) Removal of
588 copper improves the lipid content in *Nannochloropsis oculata* culture. Environ Sci Pollut
589 Res, 27(35): 44195-44204. https://doi.org/10.1007/s11356-020-10283-4
590 Akar T, Anilan B, Gorgulu A, et al (2009) Assessment of cationic dye biosorption characteristics
591 of untreated and non-conventional biomass: *Pyracantha coccinea berries*. J Hazard Mater,
592 168:1302-1309. https://doi.org/10.1016/j.jhazmat.2009.03.011
593 Allen M M (1968) Simple Conditions for Growth of Unicellular Blue-Green Algae on Plates. J
594 Phycol, 4(1):1-4. https://doi.org/10.1111/j.1529-8817.1968.tb04667.x

595 Ashraf M A, Maah M J, Yusoff I (2014) Soil contamination, risk assessment and remediation. In
596 Environmental Risk Assessment of Soil Contamination: Vol. i (3-56).
597 https://doi.org/10.1016/j.colsurfa.2011.12.014
598 Asri M, El Ghachtouli N, Elabed S, Ibnsouda S, et al (2018) *Wicherhamomyces anomalus* biofilm
599 supported on wood husk for chromium wastewater treatment. J Hazard Mater, 359: 554–562.
600 https://doi.org/10.1016/j.jhazmat.2018.05.050
601 Belghith T, Athmouni K, Bellassoued K, et al (2016) Physiological and biochemical response of
602 *Dunaliella salina* to cadmium pollution. J Appl Phycol, 28(2):991–999.
603 https://doi.org/10.1007/s10811-015-0630-5
604 Benhima R, El Arroussi H, Kadmiri I M, et al (2018) Nitrate Reductase Inhibition Induces Lipid
605 Enhancement of *Dunaliella Tertiolecta* for Biodiesel Production. Sci World J, 2018(3).
606 https://doi.org/10.1155/2018/6834725
607 Bradford M M B (1976) Rapid and Sensitive Method for quantitation of microgram quantities of
608 protein utilizing principle of protein-dye binding. Anal Biochem, 72:248-254.
609 https://doi.org/10.1016/0003-2697(76)90527-3
610 Carfagna S, Lanza N, Salbitani G, et al (2013) Physiological and morphological responses of Lead
611 or Cadmium exposed *Chlorella sorokiniana* 211-8K (Chlorophyceae). SpringerPlus, 2(1):1-
612 7. https://doi.org/10.1186/2193-1801-2-147
613 Cheloni G, Slaveykova V I (2013) Optimization of the C11-BODIPY581/591 dye for the
614 determination of lipid oxidation in *Chlamydomonas reinhardtii* by flow cytometry.
615 Cytometry Part A, 83(10):952-961. https://doi.org/10.1002/cyto.a.22338
616 Chibueze C, Chioma A, Chikere B (2016) Bioremediation techniques-classification based on site
617 of application: principles, advantages, limitations, and prospects. World J Microbiol
618 Biotechnol, 32(11):1-18. https://doi.org/10.1007/s11274-016-2137-x

619 Chinedu O J, Justin M A, Charles M, et al (2012) Biosorption of Pb (II) and Cd (II) ions from
620 Aqueous Solution using Dead Biomass of Fresh Water Green Algae *Cosmarium panamense*.
621 Int J Chem Eng Res, 4(1):39–59.
622 da Silva T L, Santos C A, Reis A (2009) Multi-parameter flow cytometry as a tool to monitor
623 heterotrophic microalgal batch fermentations for oil production towards biodiesel.
624 Biotechnol Bioprocess Eng, 14(3):330-337. https://doi.org/10.1007/s12257-008-0228-8
625 Danouche M, El Ghachtouli N, El Baouchi, A, et al (2020) Heavy metals phycoremediation using
626 tolerant green microalgae: Enzymatic and non-enzymatic antioxidant systems for the
627 management of oxidative stress. J Environ Chem Eng, 8(5):104460. https://
628 doi.org/10.1016/j.jece.2020.104460
629 Dittami S M, Scornet D, Petit J L, et al (2009) Global expression analysis of the brown alga
630 *Ectocarpus siliculosus* (Phaeophyceae) reveals large-scale reprogramming of the
631 transcriptome in response to abiotic stress. Genome Biol, 10(6). https://doi.org/10.1186/gb-
632 2009-10-6-r66
633 Dubois M, Gilles K A, Hamilton J K, et al (1956) Colorimetric Method for Determination of Sugars
634 and Related Substances. Anal Chem, 28(3):350-356. https://doi.org/10.1021/ac60111a017
635 El Arroussi, H, Benhima R, Bennis I. et al (2015) Improvement of the potential of *Dunaliella*
636 *tertiolecta* as a source of biodiesel by auxin treatment coupled to salt stress. Renew Energy,
637 77:15-19. https://doi.org/10.1016/j.renene.2014.12.010
638 El Arroussi H, Benhima R, El Mernissi N, et al (2017) Screening of marine microalgae strains from
639 Moroccan coasts for biodiesel production. Renew Energy, 113:1515-1522.
640 https://doi.org/10.1016/j.renene.2017.07.035

641 Filimonova V, Gonçalves F, Marques J C, et al (2016) Fatty acid profiling as bioindicator of
642 chemical stress in marine organisms: A review. Ecol Indic, 67:657-672.
643 https://doi.org/10.1016/j.ecolind.2016.03.044
644 Flouty R, Estephane G (2012) Bioaccumulation and biosorption of copper and lead by a unicellular
645 algae *Chlamydomonas reinhardtii* in single and binary metal systems: A comparative study.
646 J Environ Manage, 111:106-114. https://doi.org/10.1016/j.jenvman.2012.06.042
647 Garrett R G (2000) Natural sources of metals to the environment. Hum Ecol Risk Assess, 6(6):945-
648 963. https://doi.org/10.1080/10807030091124383
649 Guschina I A, Harwood J L (2006) Lead and copper effects on lipid metabolism in cultured lichen
650 photobionts with different phosphorus status. Phytochemistry, 67(16):1731-1739.
651 https://doi.org/10.1016/j.phytochem.2006.01.023
652 Hadjoudja S, Deluchat V, Baudu M (2010) Cell surface characterisation of *Microcystis aeruginosa*
653 and *Chlorella vulgaris*. J Colloid Interface Sci, 342(2):293-299.
654 https://doi.org/10.1016/j.jcis.2009.10.078
655 Han S F, Jin W, Abomohra A E F, et al (2019) Municipal Wastewater Enriched with Trace Metals
656 for Enhanced Lipid Production of the Biodiesel-Promising Microalga *Scenedesmus obliquus*.
657 Bioenergy Res, 12(4):1127-1133. https://doi.org/10.1007/s12155-019-10042-5
658 Hassler C S, Slaveykova V I, Wilkinson, K J (2004) Discriminating between intra-and extracellular
659 metals using chemical extractions. Limnol Oceanogy-Meth, 2(7):237-247.
660 https://doi.org/10.4319/lom.2004.2.237
661 He J, Chen J P (2014) A comprehensive review on biosorption of heavy metals by algal biomass:
662 Materials, performances, chemistry, and modeling simulation tools. Bioresour Technol, 160:
663 67-78. https://doi.org/10.1016/j.biortech.2014.01.068

664 Jais N M, Mohamed R M S R, Al-Gheethi A A, et al (2017) The dual roles of phycoremediation
665 of wet market wastewater for nutrients and heavy metals removal and microalgae biomass
666 production. Clean Technol Environ Policy, 19(1):37-52. https://doi.org/10.1007/s10098-
667 016-1235-7
668 Jara A De, Martel A, Molina C, et al (2003) Flow cytometric determination of lipid content in a
669 marine dinoflagellate, *Crypthecodinium cohnii*. J Appl Phycol, 15:433-438.
670 https://doi.org/10.1023/A:1026007902078
671 Jena J, Pradhan N, Aishvarya V, et al (2015) Biological sequestration and retention of cadmium as
672 CdS nanoparticles by the microalga Scenedesmus-24. J Appl Phycol, 27(6):2251-2260.
673 https://doi.org/10.1007/s10811-014-0499-8
674 Kay A R (2017) How cells can control their size by pumping ions. Front. Cell Dev. Biol, 5:1-14.
675 https://doi.org/10.3389/fcell.2017.00041
676 Kim B, Praveenkumar R, Lee J, et al (2016) Magnesium aminoclay enhances lipid production of
677 mixotrophic *Chlorella* sp. KR-1 while reducing bacterial populations. Bioresour Technol,
678 219:608-613. https://doi.org/10.1016/j.biortech.2016.08.034
679 Kumar K S, Dahms H U, Won E J, et al (2015) Microalgae-A promising tool for heavy metal
680 remediation. Ecotoxicol Environ Saf, 113:329-352.
681 https://doi.org/10.1016/j.ecoenv.2014.12.019
682 Lee J, Choi H, Hwang U, et al (2019) Toxic effects of lead exposure on bioaccumulation, oxidative
683 stress, neurotoxicity, and immune responses in fish: A review. Environ Toxicol Pharmacol,
684 68:101-108. https://doi.org/10.1016/j.etap.2019.03.010
685 Leong Y K, Chang J S (2020) Bioremediation of heavy metals using microalgae: Recent advances
686 and mechanisms. Bioresour Technol, 303:122886.
687 https://doi.org/10.1016/j.biortech.2020.122886

688 Li C, Zheng C, Fu H, et al (2021) Contrasting detoxification mechanisms of *Chlamydomonas*
689 *reinhardtii* under Cd and Pb stress. Chemosphere, 274:129771.
690 https://doi.org/10.1016/j.chemosphere.2021.129771
691 Li Y, Xia L, Huang R, et al (2017) Algal biomass from the stable growth phase as a potential
692 biosorbent for Pb(II) removal from water. RSC Advances, 7(55):34600–34608.
693 https://doi.org/10.1039/c7ra06749f
694 Lichtenthaler H K, Buschmann C (2001) Chlorophylls and Carotenoids: Measurement And
695 Characterization by UV-VIS Spectroscopy. Current Protocols in Food Analytical Chemistry,
696 1(1), F4-3. https://doi.org/10.1002/0471709085.ch21
697 Liu L, Pohnert G, Wei D (2016) Extracellular Metabolites from Industrial Microalgae and Their
698 Biotechnological Potential. Mar drugs, 14(10):1–19. https://doi.org/10.3390/md14100191
699 Liyanage L M M, Lakmali W G M, Athukorala S N P, et al (2020) Application of live
700 *Chlorococcum aquaticum* biomass for the removal of Pb(II) from aqueous solutions. J Appl
701 Phycol, 32(6):4069-4080. https://doi.org/10.1007/s10811-020-02242-w
702 Lu N, Wei D, Jiang X L, et al (2012) Fatty Acids Profiling and Biomarker Identification in Snow
703 Alga *Chlamydomonas Nivalis* by NaCl Stress Using GC/MS and Multivariate Statistical
704 Analysis. Anal Lett, 45(10):1172-1183. https://doi.org/10.1080/00032719.2012.673094
705 Malik A (2004) Metal bioremediation through growing cells. Environment International,
706 30(2):261-278. https://doi.org/10.1016/j.envint.2003.08.001
707 Marcilla A, Gómez-Siurana A, Gomis C, et al (2009) Characterization of microalgal species
708 through TGA/FTIR analysis: Application to *nannochloropsis* sp. Thermochim Acta, 484(1-
709 2): 41-47. https://doi.org/10.1016/j.tca.2008.12.005

710 Minhas A K, Hodgson P, Barrow C J, et al (2016) A Review on the Assessment of Stress
711 Conditions for Simultaneous Production of Microalgal Lipids and Carotenoids. Front
712 microbiol, 7(546):1-19. https://doi.org/10.3389/fmicb.2016.00546
713 Chanda M, Benhima R, El mernissi N, et al (2020) Screening of microalgae liquid extracts for their
714 biostimulant properties on plant growth, nutrient uptake and metabolite profile of *Solanum*
715 *lycopersicum* L. Sci Rep 10(282). https://doi.org/10.1038/s41598-020-59840-4
716 Nanda M, Kumar K, Kumar V (2021) Micro-pollutant Pb(II) mitigation and lipid induction in
717 oleaginous microalgae *Chlorella sorokiniana* UUIND6. Environ Technol Innov, 23, 101613.
718 https://doi.org/10.1016/j.eti.2021.101613
719 Napan K, Teng L, Quinn J C, et al (2015) Impact of heavy metals from flue gas integration with
720 microalgae production. Algal Res, 8:83-88. https://doi.org/10.1016/j.algal.2015.01.003
721 Navakoudis A M E, Ververidis K P F (2018) Microalgae: a potential tool for remediating aquatic
722 environments from toxic metals. Int J Environ Sci Technol, 15(8):1815-1830.
723 https://doi.org/10.1007/s13762-018-1783-y
724 Nazari F, Movafeghi A, Jafarirad S, et al (2018) Synthesis of Reduced Graphene Oxide-Silver
725 Nanocomposites and Assessing Their Toxicity on the Green Microalga *Chlorella vulgaris*.
726 BioNanoScience, 8(4):997-1007. https://doi.org/10.1007/s12668-018-0561-0
727 Olofsson M, Lamela T, Nilsson E, et al (2012) Seasonal variation of lipids and fatty acids of the
728 microalgae *Nannochloropsis oculata* grown in outdoor large-scale photobioreactors.
729 Energies, 5(5), 1577–1592. https://doi.org/10.3390/en5051577
730 Ozkan A, Berberoglu H (2013) Physico-chemical surface properties of microalgae. Colloids Surf.
731 B, 112:287-293. https://doi.org/10.1016/j.colsurfb.2013.08.001

732 Pérez-Rama M, Abalde Alonso J, Herrero López C, et al (2002) Cadmium removal by living cells
733 of the marine microalga *Tetraselmis suecica*. Bioresour Technol, 84(3):265-270.
734 https://doi.org/10.1016/S0960-8524(02)00045-7
735 Pham T-L, Dao T-S, Bui H, et al (2020) Lipid Production Combined with Removal and
736 Bioaccumulation of Pb by *Scenedesmus* sp. Green Alga. Pol J Environ Stud, 29(2):1785-
737 1791. https://doi.org/10.15244/pjoes/109277
738 Piotrowska-Niczyporuk A, Bajguz A, Talarek M, et al (2015) The effect of lead on the growth,
739 content of primary metabolites, and antioxidant response of green alga *Acutodesmus obliquus*
740 (Chlorophyceae). Environ Sci Pollut Res, 22(23):19112-19123.
741 https://doi.org/10.1007/s11356-015-5118-y
742 Rai U N, Singh N K, Upadhyay A K, et al (2013) Chromate tolerance and accumulation in
743 *Chlorella vulgaris* L.: Role of antioxidant enzymes and biochemical changes in
744 detoxification of metals. Bioresour Technol, 136:604-609.
745 https://doi.org/10.1016/j.biortech.2013.03.043
746 Randrianarison G, Ashraf M A (2017) Microalgae: a potential plant for energy production.
747 Geology, Ecology, and Landscapes, 1(2):104-120.
748 https://doi.org/10.1080/24749508.2017.1332853
749 Richmond A (2004) Economic Applications of Microalgae. In Handbook of Microalgal Culture:
750 Applied Phycology and Biotechnology, (255–353).
751 https://doi.org/10.1002/9781118567166.ch1
752 Rocchetta I, Mazzuca M, Conforti V, et al (2012) Chromium induced stress conditions in
753 heterotrophic and auxotrophic strains of *Euglena gracilis*. Ecotoxicol Environ Saf, 84:147-
754 154. https://doi.org/10.1016/j.ecoenv.2012.07.020

Rocchetta I, Mazzuca M, Conforti V, et al (2006) Effect of chromium on the fatty acid composition of two strains of *Euglena gracilis*. Environ Pollut, 141(2):353-358. https://doi.org/10.1016/j.envpol.2005.08.035

Romero N, Visentini F F, Márquez V E, et al (2020) Physiological and morphological responses of green microalgae *Chlorella vulgaris* to silver nanoparticles. Environ Res, 189. 109857. https://doi.org/10.1016/j.envres.2020.109857

Saavedra R, Muñoz R, Taboada M E, et al (2018) Comparative uptake study of arsenic, boron, copper, manganese and zinc from water by different green microalgae. Bioresour Technol, 263:49-57. https://doi.org/10.1016/j.biortech.2018.04.101

Samadani M, Perreault F, Oukarroum A, et al (2018) Effect of cadmium accumulation on green algae *Chlamydomonas reinhardtii* and acid-tolerant *Chlamydomonas* CPCC 121. Chemosphere, 191:174-182. https://doi.org/10.1016/j.chemosphere.2017.10.017

Selvi A, Rajasekar A, Theerthagiri J, et al (2019) Integrated remediation processes toward heavy metal removal/recovery from various environments-A review. Front environ sci, 7:66. https://doi.org/10.3389/fenvs.2019.00066

Sibi G, Anuraag T S, Bafila G (2014) Copper stress on cellular contents and fatty acid profiles in *Chlorella* species. Online J Biol Sci, 14(3):209-217. https://doi.org/10.3844/ojbsci.2014.209.217

Singh D V, Bhat R A, Upadhyay A K, et al (2021) Microalgae in aquatic environs: A sustainable approach for remediation of heavy metals and emerging contaminants. Environ Technol Innov, 21:101340. https://doi.org/10.1016/j.eti.2020.101340

Sorigué D, Légeret B, Cuiné S, et al (2016) Microalgae synthesize hydrocarbons from long-chain fatty acids via a light-dependent pathway. Plant Physiol, 171(4):2393-2405. https://doi.org/10.1104/pp.16.00462

779 Sudhakar K, Premalatha M (2015) Characterization of micro algal biomass through FTIR/TGA
780 /CHN analysis: Application to *Scenedesmus* sp. Energy Sources, Part A: Recovery,
781 Utilization and Environmental Effects, 37(21):2330-2337.
782 https://doi.org/10.1080/15567036.2013.825661
783 Suman T Y, Radhika Rajasree S R, Kirubagaran R (2015) Evaluation of zinc oxide nanoparticles
784 toxicity on marine algae *Chlorella vulgaris* through flow cytometric, cytotoxicity and
785 oxidative stress analysis. Ecotoxicol Environ Saf, 113:23-30.
786 https://doi.org/10.1016/j.ecoenv.2014.11.015
787 Tahira S, Khan S, Samrana S, et al (2019) Bio-assessment and remediation of arsenic (arsenite As-
788 III) in water by *Euglena gracilis*. J Appl Phycol, 31(1):423-433.
789 https://doi.org/10.1007/s10811-018-1593-0
790 Thomas M K, Fontana S, Reyes M, et al (2018) Quantifying cell densities and biovolumes of
791 phytoplankton communities and functional groups using scanning flow cytometry, machine
792 learning and unsupervised clustering. PLoS ONE, 13(5):1-22.
793 https://doi.org/10.1371/journal.pone.0196225
794 Tran N H, You S, Hosseini-bandegharaei A (2017) Mistakes and inconsistencies regarding
795 adsorption of contaminants from aqueous solutions: A critical review. Water Res, 120:88-
796 116. https://doi.org/10.1016/j.watres.2017.04.014
797 Urrutia C, Yañez-Mansilla E, Jeison D (2019) Bioremoval of heavy metals from metal mine
798 tailings water using microalgae biomass. Algal Res, 43:101659.
799 https://doi.org/10.1016/j.algal.2019.101659
800 USEPA (2016). National Primary Drinking Water Regulations. in: EPA 816-F-09-004, (Ed.)
801 U.S.E.P. Agency, United State Environmental Protection Agency. United State. Drinking
802 Water Contaminants, 141–142. https://doi.org/EPA 816-F-09-004

803 Van den Berg R A, Hoefsloot H C J, Westerhuis J A, et al (2006) Centering, scaling, and
804 transformations: Improving the biological information content of metabolomics data. BMC
805 Genomics, 7:1-15. https://doi.org/10.1186/1471-2164-7-142
806 Van Oss C J, Chaudhury M K, Good R J (1988) Interfacial Lifshitz-van der Waals and polar
807 interactions in macroscopic systems. Chem Rev, 88(6):927-941.
808 https://doi.org/10.1021/cr00088a006
809 Venkata Mohan S, Ramanaiah S V, Rajkumar B, et al (2007) Removal of fluoride from aqueous
810 phase by biosorption onto algal biosorbent *Spirogyra* sp.-IO2: Sorption mechanism
811 elucidation. J Hazard Mater, 141(3):465-474. https://doi.org/10.1016/j.jhazmat.2006.07.008
812 Vichi S, Gallardo-chacón J J, Pradelles R, et al (2010) Surface properties of *Saccharomyces*
813 *cerevisiae* lees during sparkling wine ageing and their effect on flocculation. Int J Food
814 Microbiol, 140(2–3):125-130. https://doi.org/10.1016/j.ijfoodmicro.2010.04.009
815 Vogler E A (1998). Structure and reactivity of water at biomaterial surfaces. Adv Colloid Interface
816 Sci, 74:69-117. https://doi.org/10.1016/S0001-8686(97)00040-7
817 Volkman J K (2016) Sterols in Microalgae. The Physiology of Microalgae. In Developments in
818 Applied Phycology 6 (pp. 485–505). https://doi.org/DOI 10.1007/978-3-319-24945-2_19
819 Wollmann F, Dietze S, Ackermann J U, et al (2019). Microalgae wastewater treatment: Biological
820 and technological approaches. Eng Life Sci, 19(12):860-871.
821 https://doi.org/10.1002/elsc.201900071
822 Wychen S Van, Laurens L M L (2017) Total Carbohydrate Content Determination of Microalgal
823 Biomass by Acid Hydrolysis Followed by Spectrophotometry or Liquid Chromatography. In
824 Methods in Molecular Biology (257–284). https://doi.org/10.1007/7651_2017_106
825 Xia L, Huang R, Li Y, et al (2017) The effect of growth phase on the surface properties of three
826 oleaginous microalgae (*Botryococcus* sp. FACGB-762, *Chlorella* sp. XJ-445 and

827 *Desmodesmus bijugatus* XJ-231). PLoS ONE, 12(10).
828 https://doi.org/10.1371/journal.pone.0186434
829 Yalçin E, Çavuşoğlu K, Kinalioğlu K (2010) Biosorption of Cu2+ and Zn2+ by raw and autoclaved
830 *Rocella phycopsis*. J Environ Sci (China), 22(3):367-373. https://doi.org/10.1016/S1001-
831 0742(09)60117-0
832 Yan X, Liu M, Zhong J, et al (2018) How human activities affect heavy metal contamination of
833 soil and sediment in a long-term reclaimed area of the Liaohe River Delta, North China.
834 Sustainability (Switzerland), 10(2):1-19. https://doi.org/10.3390/su10020338
835 Ying Z T, Dobbs F C (2007) Green autofluorescence in dinoflagellates, diatoms, and other
836 microalgae and its implications for vital staining and morphological studies. Appl Environ
837 Microbiol, 73(7):2306-2313. https://doi.org/10.1128/AEM.01741-06
838 Zehra T, Priyantha N, Lim L B L (2016) Removal of crystal violet dye from aqueous solution using
839 yeast-treated peat as adsorbent: thermodynamics, kinetics, and equilibrium studies. Environ
840 Earth Sci, 75(4):1-15. https://doi.org/10.1007/s12665-016-5255-8
841 Zheng H, Guo W, Li S, et al (2016) Biosorption of cadmium by a lipid extraction residue of lipid-
842 rich microalgae. RSC Advances, 6(24):2005-20057. https://doi.org/10.1039/c5ra27264e
843 Zhou G J, Peng F Q, Zhang L J, et al (2012) Biosorption of zinc and copper from aqueous solutions
844 by two freshwater green microalgae *Chlorella pyrenoidosa* and *Scenedesmus obliquus*.
845 Environ. Sci Pollut Res, 19(7):2918-2929. https://doi.org/10.1007/s11356-012-0800-9

# Figures

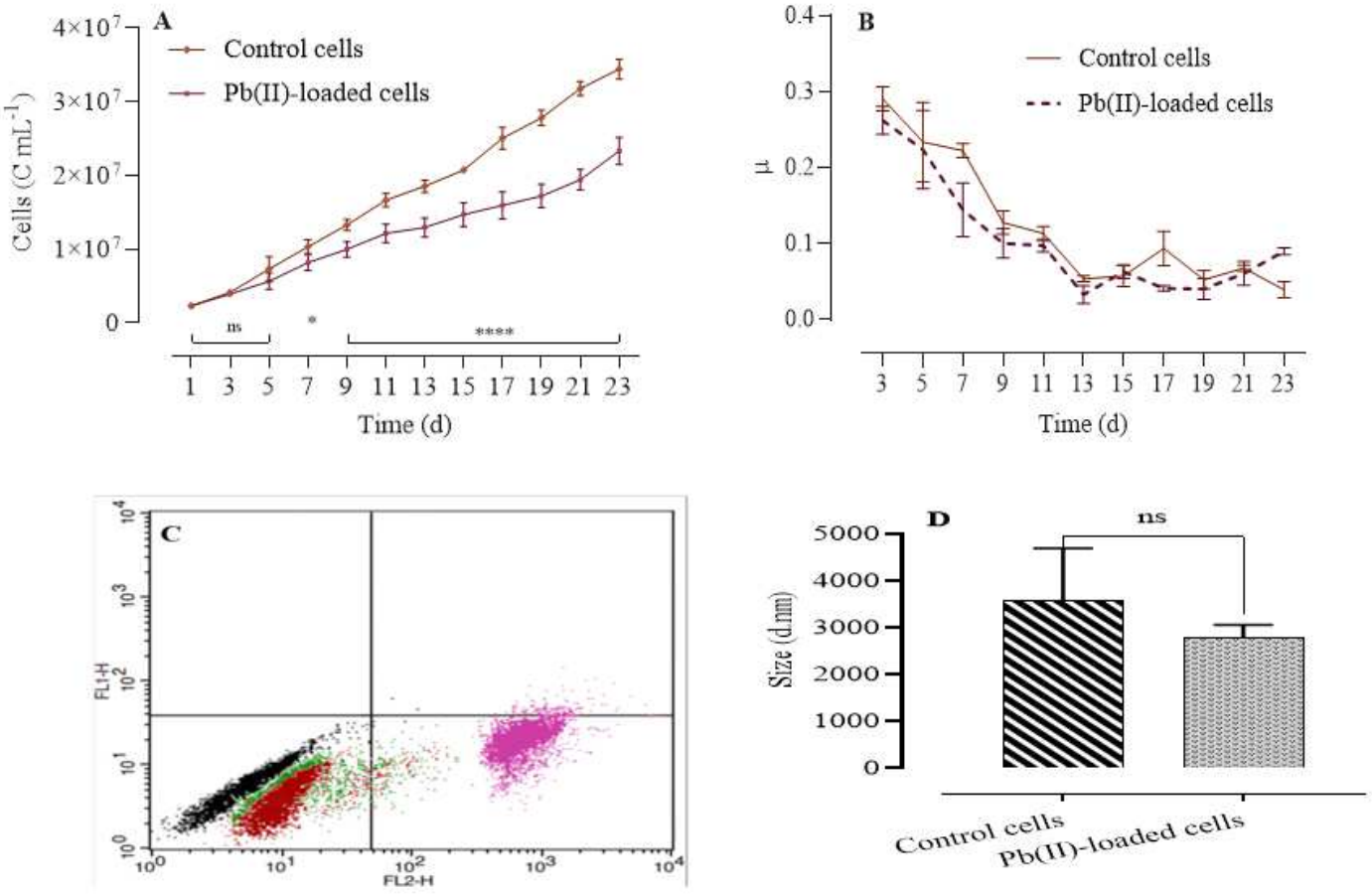


**Figure 1**

Shows growth kinetics (A), specific growth rate (B) of S. obliquus cultures in control and Pb(II)-doped medium. Fig. 1C illustrate the cytogram of the cells viability: (black) cells auto-fluorescence canceled (green) the negative control (96.07%), (red) after Pb(II)-phycoremediation (90.1%) and (pink) heat-inactivated cells. The population moved in the FL2 channel corresponding to the positive control (0.07%). UL: Upper Left, UR: Upper Right, LL: Lower Left, LR: Lower Right. Fig. 1D displays the effect of Pb(II) ions on the intensity particle size distribution of cells.

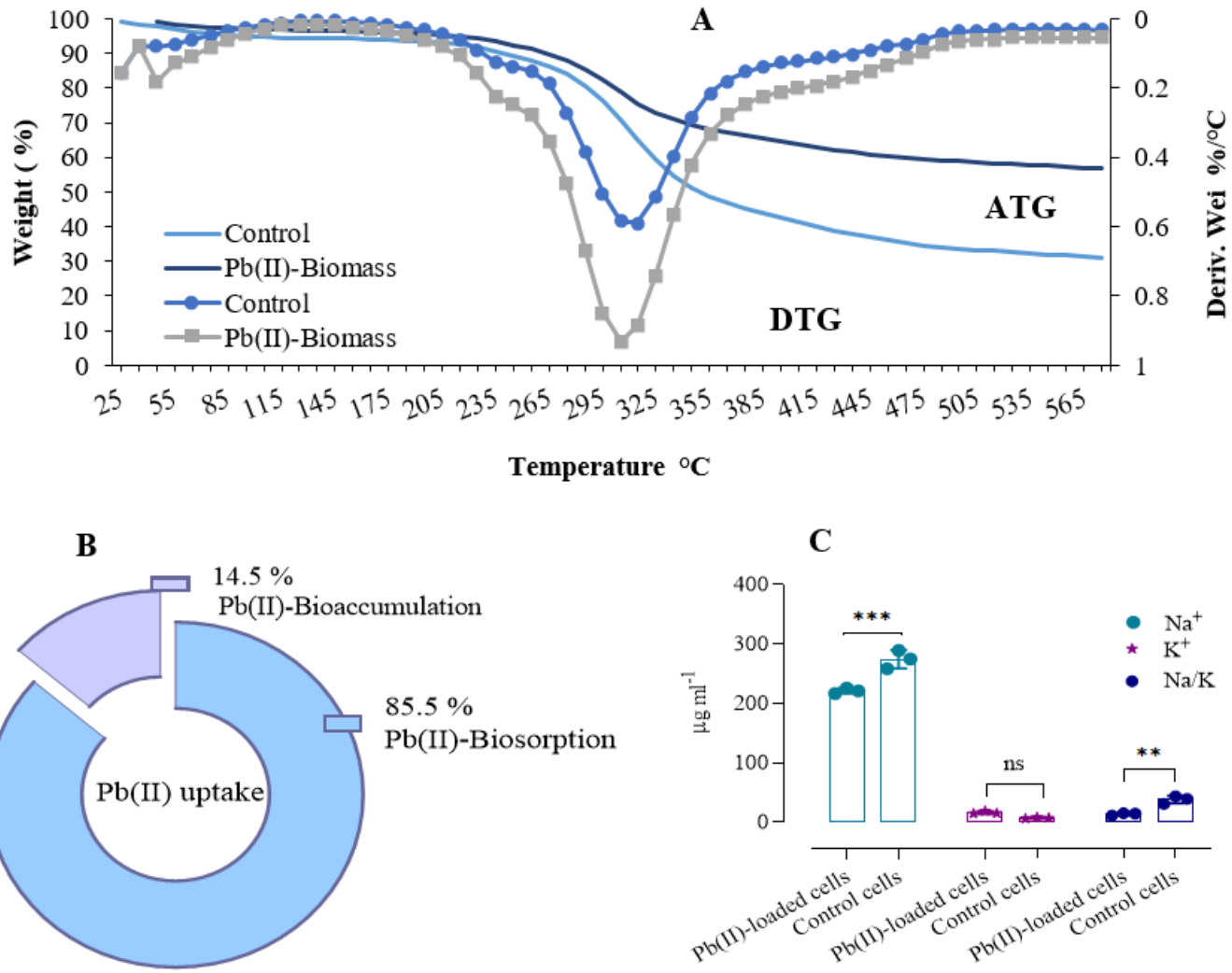


## Figure 2

(A). plots the TGA and DTG profile of the decomposition of controlled and Pb(II)-loaded cells, (B) illustrates the rate of bioaccumulation and biosorption of Pb (II) ions by cells of S. obliquus, and (C) displays the contents of Na+, K+ and the ratios of Na/K in control and Pb(II)-loaded cells.

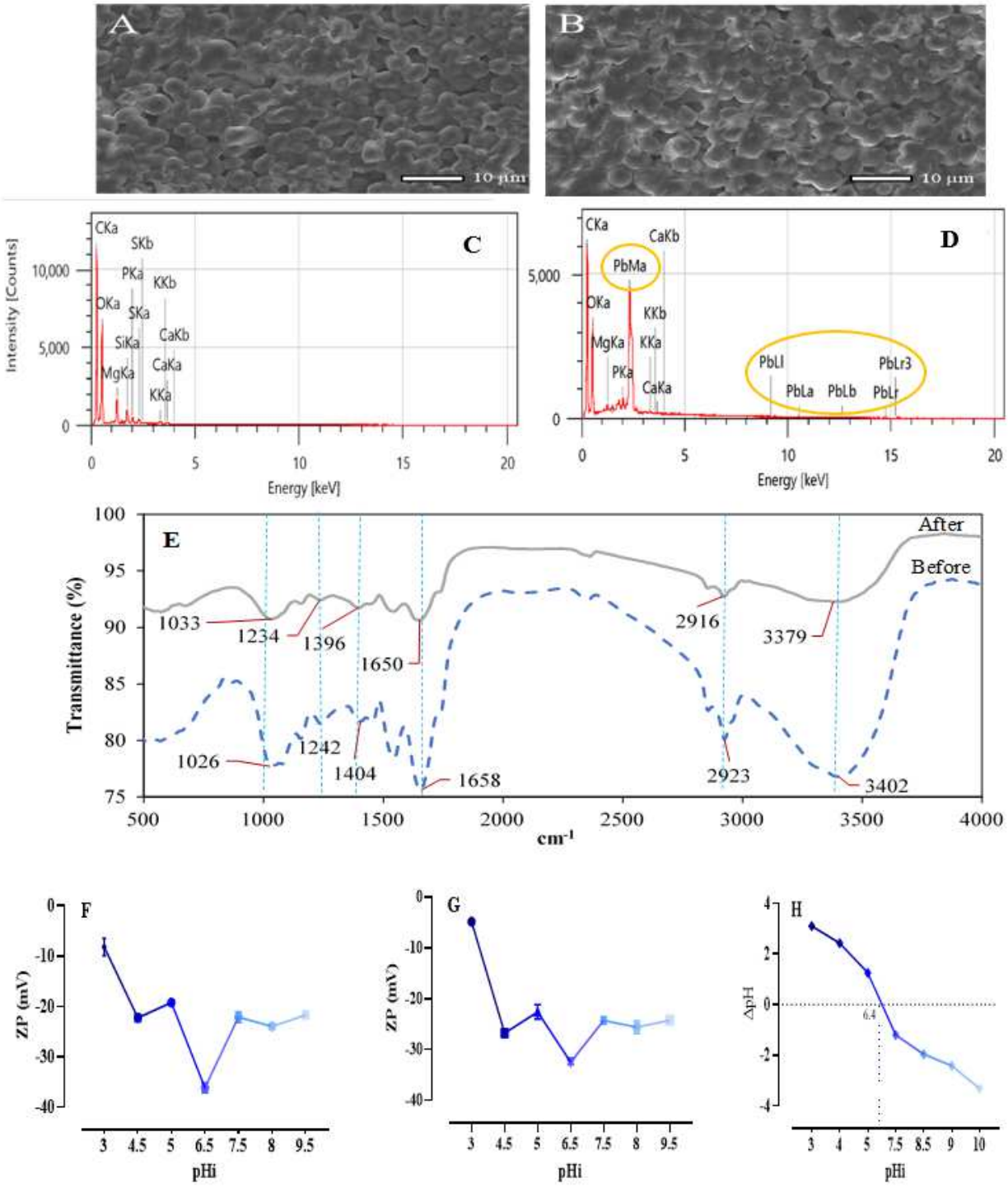


## Figure 3

Displays SEM image of (A) control cells; (B) Pb(II)-loaded cells at x8000 magnification. as well as the selected X-ray spectra of control (C), Pb(II)-loaded cells (D), FTIR spectra of control and Pb(II)-loaded cells (E), zeta potential of control (F) and Pb(II)-loaded cells (G), as well as zero pH loading (H) of S. obliquus biomass in the pHi range of 3-10.

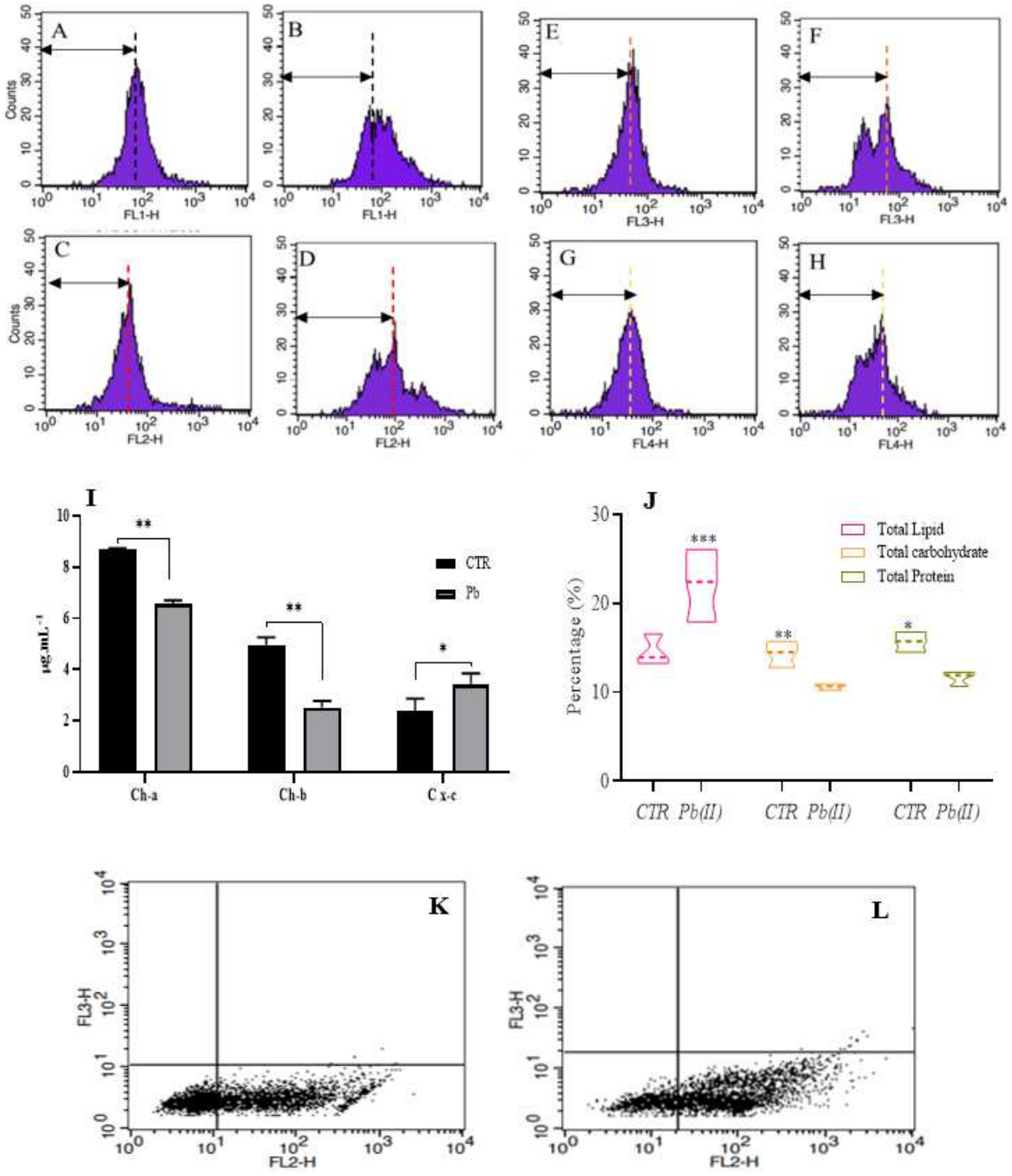


## Figure 4

shows the autofluorescence of native pigments of control cells (A, C, E and G) and (B, D, F and H) and Pb(II)-loaded cells. Fig 4 I illustrate the concentration of chlorophyll a (Ch-a), b (Ch-b), and total carotenoids (C x+c) in control (CTR) and Pb(II)-loaded cells. Fig 4 (J) shows the compositions of the total lipid, carbohydrate and protein in control and Pb(II)-loaded cells. Fig 4 (K) and (L) present respectively the NR staining dot plots of control and Pb(II)-loaded cells.

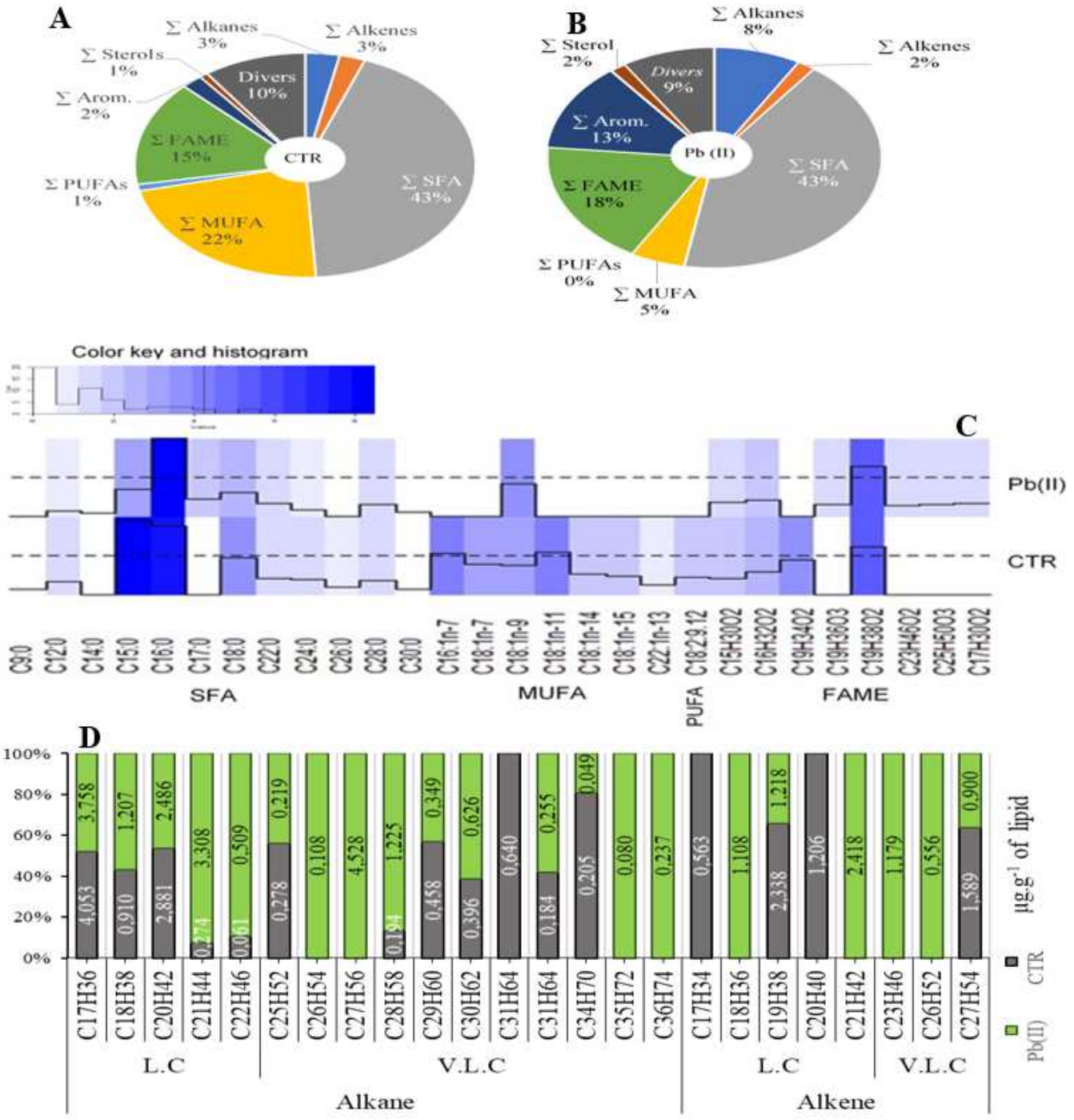


## Figure 5

indicates the level of the metabolite classes (Σ alkanes, Σ alkenes, Σ sterols, Fatty acid methyl ester (FAME); monounsaturated fatty acids (MUFA); saturated fatty acids (SFA); Polyunsaturated fatty acids (PUFA); Aromatic compounds (Arom.); divers compounds (Divers)) in control (A) and Pb(II)-loaded (B) cells. Fig. 5C shows the distribution of the fatty acid profile (fatty acid methyl ester (FAME); monounsaturated fatty acids (MUFA); saturated fatty acids (SFA); polyunsaturated fatty acids (PUFA)),

and Fig. 5D illustrates the metabolomic profiling of alkanes and alkenes (very long-chain alkanes (V.L.C); long-chain alkanes (L.C)) in control and Pb(II)-loaded cells.

## Supplementary Files

This is a list of supplementary files associated with this preprint. Click to download.

- Graphicalabstract.pptx
- Tables.pdf